Journal of Materials Chemistry C

Accepted Manuscript

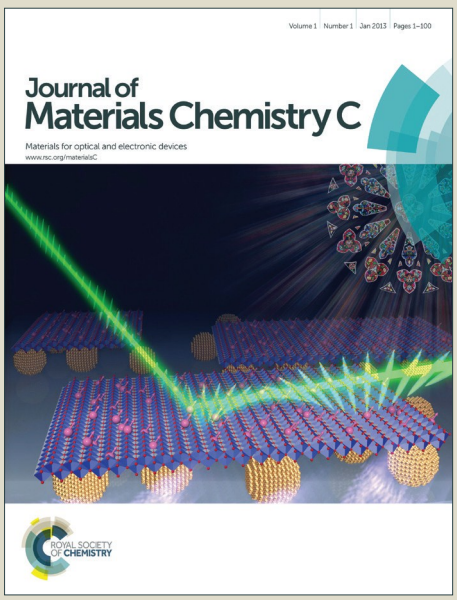

ROYAL SOCIETY OF CHEMISTRY

www.rsc.org/materialsC

Journal of Materials Chemistry C

RSCPublishing

ARTICLE

The nano-crystallization and fluorescence of terbium doped $Na_2O/K_2O/CaO/CaF_2/Al_2O_3/SiO_2$ glasses

Cite this: DOI: 10.1039/x0xx00000x

Christian Bocker*, Andreas Herrmann, Peter Loch and Christian Rüssel

Received 00th January 2012,
Accepted 00th January 2012

DOI: 10.1039/x0xx00000x

www.rsc.org/

Oxyfluoride glasses with the molar composition 59.3 SiO_2·3.7 Al_2O_3·12.3 CaO·5.3 K_2O·9.0 Na_2O·10.4 CaF_2 were doped with different Tb^{3+}-concentrations ($1\cdot10^{19}$, $5\cdot10^{19}$ and $1\cdot10^{20}$ cm^{-3}). The glasses were thermally treated in the temperature range from 550 to 600 °C, which resulted in the crystallization of cubic CaF_2. The XRD-patterns showed extremely broadened lines attributed to mean crystallite sizes in the range from 11 to 15 nm. SEM and TEM micrographs showed polycrystalline particles with a size of around 200 nm which are composed of smaller, about 15 nm large, crystallites. Static fluorescence spectra as well as fluorescence decay curves were recorded for samples with different TbF_3-concentrations and different thermal treatment. For samples with a low Tb^{3+} doping concentration notably prolonged fluorescence lifetimes were measured.

Introduction

In the past few years, much attention has been paid to Tb^{3+} doped glasses due to their optical properties which are advantageous for numerous applications [1-4]. If the chemical composition of oxyfluoride glass-ceramics is carefully tailored, thermal treatment at temperatures slightly above the glass transition temperature T_g, results in the precipitation of fluorides. Here, the formation of rare earth or alkaline earth fluorides such as LaF_3, $NaGd(La)F_4$, CaF_2, SrF_2 and BaF_2 have been described in the literature [5-11]. Especially in the CaF_2 lattice, rare earth fluorides, such as Yb^{3+}, Er^{3+} and Tm^{3+} can be incorporated which may lead to enhanced fluorescence lifetimes [12-14]. Among the potential applications, up-conversion and laser materials are to be mentioned. Glass-ceramics containing alkaline earth fluoride nanocrystals doped with rare earth ions may enable the combination of advantageous properties of glasses (possibility to draw fibre) with those of crystals (improved fluorescence properties). This may lead to challenging new materials suitable e.g. as fibre amplifiers [15-17].

The general problem of multi-phase optical materials is light scattering. Light scattering is observed, if two phases with different refractive indices occur and if the dimensions of these phase changes are not very small in comparison to the wavelength of the used light. If light scattering has to be avoided, either the refractive indices of the occurring phases have to be identical at all relevant wavelengths and temperatures or the crystallite sizes must be much smaller than the wavelength of the light used. Furthermore, the crystal size distribution plays an important part; it must be narrow in order to avoid light scattering because otherwise the largest particles give rise to scattering.

In the past decade, a general route for the preparation of transparent glass-ceramics was described in the literature. It was shown for many compositions that the viscosity increases during the course of the crystallization of fluorides from a silicate glass [18, 19]. Near the crystal, the glass composition is depleted in crystal forming components. This results in an enrichment of the network forming SiO_2 in this layer. Hence the viscosity is notably increased within this layer which consequently acts as a diffusion barrier. A first experimental hint for a change in viscosity of the residual glassy phase during the course of crystallization is the measured increase of the glass transition temperature with increasing annealing time. This behavior was experimentally observed during the crystallization of fluorides from many glass compositions. That means a diffusion gradient is formed around the crystal. Furthermore also the diffusion coefficient decreases drastically and hence the crystal growth velocity decreases much more than expected from a simple process with constant diffusion coefficients. The occurrence of such layers in the meantime has been proved using anomalous X-ray scattering (ASAXS) and advanced transmission electron microscopic techniques [20-22]. In the case of the relatively stable BaF_2, high resolution TEM including EELS studies could be carried out using a comparatively low acceleration voltage [23]. In the case of CaF_2, TEM studies are very difficult to conduct even using aberration corrected TEM and low acceleration voltages (80 kV), because the formed fluoride crystals in the glass matrix are highly sensitive to radiation damage.

This work presents a study on the preparation, and optical properties of oxyfluoride glasses doped with Tb^{3+}-concentrations in the range from $1\cdot10^{19}$ to $1\cdot10^{20}$ cm^{-3}. The glasses are crystallized and the resulting microstructures characterized and correlated with the fluorescence properties.

Experimental

Glasses with the mol% composition 59.3 SiO_2·3.7 Al_2O_3·12.3 CaO·5.3 K_2O·9.0 Na_2O·10.4 CaF_2 were melted from reagent grade raw materials Al_2O_3, $CaCO_3$, K_2CO_3, Na_2CO_3, SiO_2 and CaF_2 in batches of 200 g in a

Table 1. The as weighed glass composition of the prepared samples.

Sample	Tb^{3+} concentration	Glass composition in mol%						
	in cm^{-3}	SiO_2	CaO	Na_2O	K_2O	Al_2O_3	Sb_2O_3	CaF_2
A0	0	59.3	12.3	9.0	5.3	3.7	0	10.4
A1	$1 \cdot 10^{19}$	59.3	12.3	9.0	5.3	3.7	0.02	10.4
A5	$5 \cdot 10^{19}$	59.3	12.3	9.0	5.3	3.7	0.02	10.4
A10	$1 \cdot 10^{20}$	59.3	12.3	9.0	5.3	3.7	0.02	10.4
B1	$1 \cdot 10^{19}$	59.3	22.7	9.0	5.3	3.7	0	0
B5	$5 \cdot 10^{19}$	59.3	22.7	9.0	5.3	3.7	0	0

platinum crucible at 1400 °C, fining for 45 min and stirred additionally 45 min at 1350 °C in an induction furnace. A glass without Tb^{3+}-doping and without the fining agent Sb_2O_5 was melted as well as three glasses with the fining agent Sb_2O_5 and increasing Tb^{3+}-concentrations ($1 \cdot 10^{19}$, $5 \cdot 10^{19}$ and $1 \cdot 10^{20}$ cm^{-3}) by adding the raw material TbF_3. Additionally, two glasses without fluoride but with the same molar ratio of cations (samples B1 and B5) doped with $1 \cdot 10^{19}$ and $5 \cdot 10^{19}$ Tb^{3+} cm^{-3} using Tb_2O_3 as raw material were prepared (see Table 1).

The melts were cast on a copper block and placed in a furnace preheated to 520 °C. Then the furnace was switched off and the samples were allowed to cool. The cooling rate of the used furnace is about 3 $K \cdot min^{-1}$ in the beginning and decreases non-linearly to 0.5 $K \cdot min^{-1}$ after approximately 4 h. Fluorine analyses by energy dispersive X-ray spectroscopy (EDS) in the scanning electron microscope showed a fluorine loss of about 10 % during melting and casting of the glass under the conditions supplied.

The samples were thermally treated at temperatures in the range from 520 to 600 °C for 20 to 60 h. In order to determine T_g and the crystallization temperature(s), the samples were powdered to a grain-size fraction of 250 to 315 µm and studied by differential scanning calorimetry (DSC 822, Mettler Toledo GmbH, Greifensee, Schweiz) as well as differential thermal analysis (Shimadzu DTA 50). XRD patterns were recorded from thermally annealed and subsequently powdered samples using X-ray diffraction (XRD, D 5000, (Siemens) Bruker AXS GmbH, Karlsruhe, Germany) with $Cu_{K\alpha}$ radiation and Bragg-Brentano geometry. Selected crystallized samples were studied by scanning electron microscopy (SEM; JSM7001F, Jeol Ltd., Tokyo, Japan) and analysed by energy dispersive X-ray spectroscopy (EDS; AMETEK GmbH, EDAX Division, Wiesbaden, Germany). For SEM imaging, the samples were etched for 10 to 20 s, using diluted hydrofluoric acid (HF, 5 %) and coated with carbon (Auto 306; Edwards, Crawley, UK) by evaporation in high vacuum (10^{-3} Pa). After etching the sample surface with HF, an exposed particle structure was observed. These particles were extracted using an extraction replica technique. Here, the coated carbon membrane is floated on diluted acid (HF) while creeping between the membrane and substrate surface and etching the latter one. The carbon film was transferred to a copper grid and studied by transmission electron microscopy (TEM; H8100, Hitachi High-Tech, Tokyo, Japan) at 200 kV and analyzed by EDS (Link ISIS 200, Oxford Instruments plc, Abingdon, UK).

Fluorescence spectra were recorded using the spectrometer (RF-5301 PC, Shimadzu Deutschland GmbH, Duisburg, Germany) in the wavelength range of 220 to 900 nm (spectral resolution: 0.2 nm). For this measurement polished samples with a thickness of 10 mm were used. The emission spectra were obtained using an excitation wavelength of about 377 nm. Fluorescence lifetimes were measured using a home-made experimental setup. For excitation of the glass samples, a high intensity pulsed InGaN-diode (LED 360-66-60-110, Roithner Lasertechnik GmbH, Wien, Austria) with an emission wavelength of 360 nm was used. The emitted fluorescence light was collected and focused by a lens array onto the entrance slit of a monochromator (H.25, HORIBA Jobin Yvon, France). The spectrum-sliced light is amplified by a photomultiplier tube (R5929, Hamamatsu Photonics K.K., Japan) connected to a digital storage oscilloscope (TDS2012, TEKTRONIX, USA). This setup enables wavelength specific lifetime measurements. Fluorescence lifetimes were measured for the strongest fluorescence transition of Tb^{3+} at around 435 and 545 nm.

Results

The as casted glasses were clear and visually transparent. The attributed XRD-patterns do not show any hint at a crystalline phase (see Figure 1, sample A0). The glass transition temperature of sample A0 as determined by DSC is 520 °C (not shown). At the temperature of 731 °C, an exothermic peak occurs due to crystallization. Furthermore, Figure 1 shows patterns recorded from samples thermally treated at 550 (T_g + 30 K), 570 (T_g + 50 K), 580 (T_g + 60 K) and 590 °C (T_g + 70 K) for 20 h. Here, strongly broadened lines at 2θ values of 28°, 47.5° and 56° all attributed to cubic calcium fluoride JCPDS-file (00-035-0815) are observed.

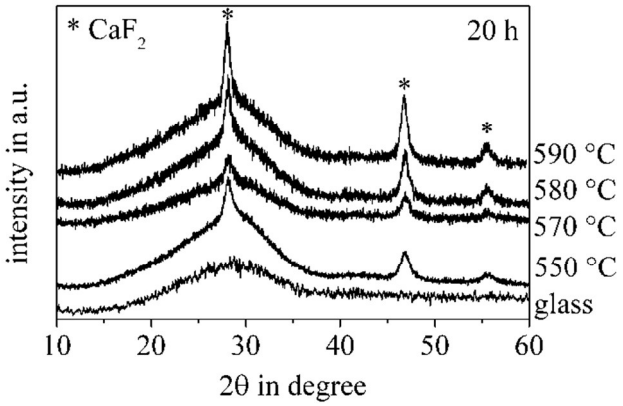

Figure 1. XRD-patterns of the undoped glass A0 crystallized at different temperatures for 20 h. The asterisks mark the peaks attributed to CaF_2.

The peak broadening is attributed to a crystallite size in the nanometer scale. Hence, the average crystallite size can be calculated using Scherrer's equation. In this case the broadened

peak at 2θ = 47.5° was selected. As shown in Figure 2, the sample annealed at 550 °C shows an average crystallite size of 11.4 nm while the size increases slightly to 13 nm for the sample annealed at 590 °C.

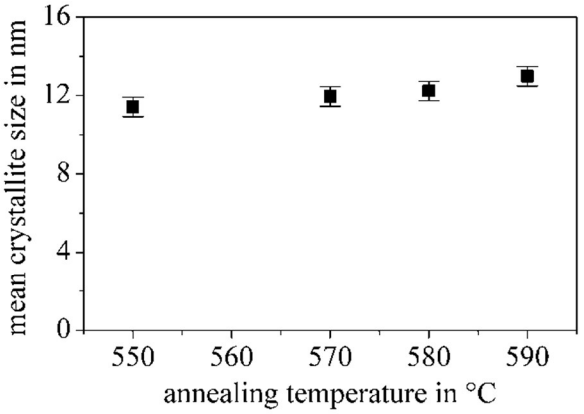

Figure 2. Crystallite sizes as a function of the annealing temperature of the undoped sample A0.

Samples annealed at temperatures in the range from 530 to 590 °C for 20 h were also studied using DSC. This enables to determine the glass transition temperature of the residual glassy phase. The glass transition temperatures for annealed samples as determined by DSC are shown in Figure 3. If the glass is annealed at 530 °C, T_g increased slightly to 525 °C in comparison to the glass without annealing. Crystallizing at 550 °C resulted in a T_g of 540 °C, whereas crystallizing at 580 °C led to a T_g of 560 °C. The accuracy of the measurement is estimated to be within ±3 K.

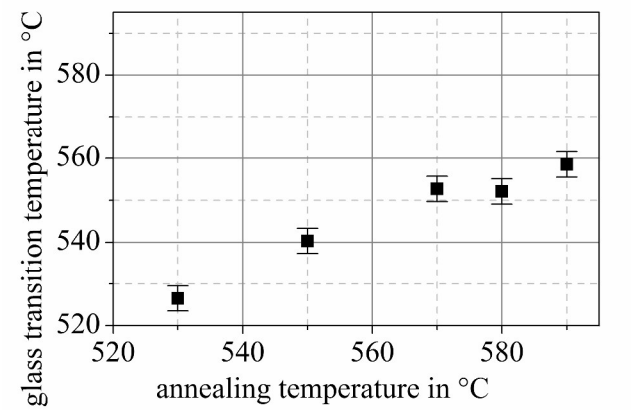

Figure 3. Glass transition temperature as a function of the annealing temperature (annealing time 20 h) of the undoped sample A0.

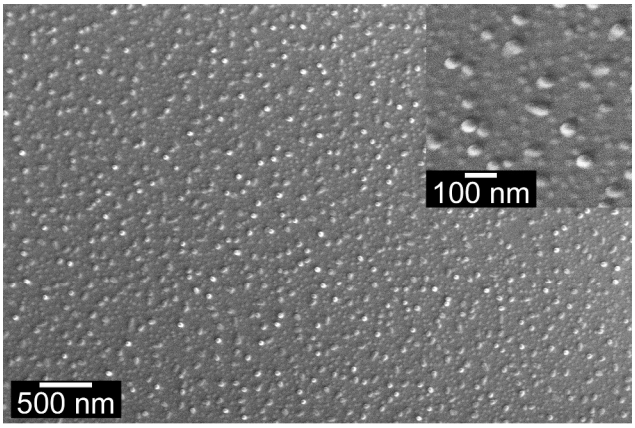

Figure 4. SEM-micrograph of sample A1 annealed at 580 °C for 20 h. The inset shows a higher magnification. The surface was polished and subsequently etched with HF.

Figure 4 shows SEM micrographs of the etched surface of sample A1 doped with $1 \cdot 10^{19}$ cm^{-3} terbium ions and annealed at 580 °C for 20 h. Homogeneously distributed particles with diameters of around 30 to 40 nm are observed. Smaller particles with less contrast can be noticed which is supposedly due to the particles that are not exposed completely by the etching routine, i.e. that stay mainly beneath the surface.

The SEM micrographs in Figure 5 show the etched surface of sample A5 doped with $5 \cdot 10^{19}$ cm^{-3} terbium ions and annealed at 580 °C for 20 h. Here also a particular microstructure is observed. The micrograph was recorded using a tilt angle of 70° providing a three-dimensional impression. Many spherical particles with a bright appearance and sizes of around 400 nm are observed. It seems that the size distribution is fairly uniform. As shown in the high resolution image as inset in Figure 5, the particles possess a substructure. EDS point analyses indicate that the particles might be enriched in fluorine in comparison to the matrix. However, a reliable quantitative EDS analysis of the particles in the SEM is difficult due to particles sizes which are much smaller than the information volume (approx. 4 µm at 15 kV). Furthermore, the pronounced topography results in uncertain geometry (position detector to sample surface) and non-linear absorption effects, especially for low energy elements, such as fluorine and sodium. Surprisingly, the microstructure of sample A5 without heat treatment is quite different. Only small circular structures with diameters in the range from 30 to 40 nm can be observed by SEM when the surface is etched by HF (not shown). It should be mentioned, that the sample without terbium (sample A0) does not show any similar microstructure. Furthermore it should be mentioned that the annealed samples of the composition A5 appear increasingly opaque after heat treatment above 550 °C.

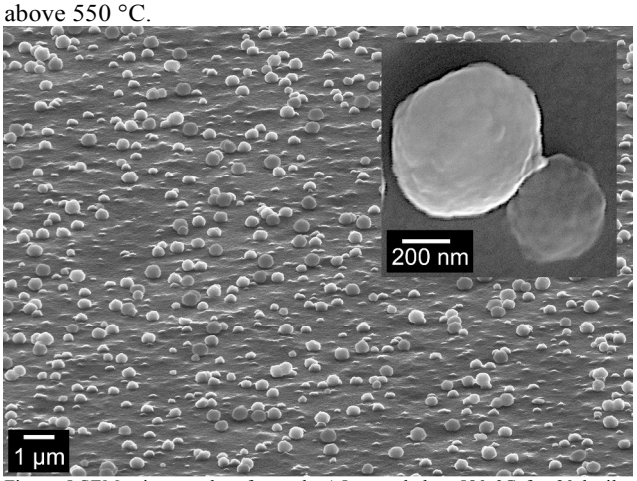

Figure 5.SEM-micrographs of sample A5 annealed at 580 °C for 20 h tilted by 70°. The inset shows two particles in high resolution without sample tilt. The surface was polished and subsequently etched by HF.

TEM analyses of the extracted particles of sample A5 annealed at 580 °C for 20 h (for preparation method: see section Experimental) were carried out. As shown in Figure 6, particles were detected which are obviously equivalent to the spherical particles observed in the SEM micrographs. In agreement with the SEM results, the particles themselves are not homogeneous. A substructure with dark appearance (due to scattering contrast) can be seen inside the spherical particles. The size of the substructure is around 15 nm which is in good agreement with the crystal sizes calculated from the XRD pattern (approx. 12

nm). Selected Area Electron Diffraction (SAD) of one particle gives evidence for the poly-crystallinity of the particles. It is remarkable that the SAD pattern exhibits distinct circular elongated spots as shown in the inset of Figure 6.

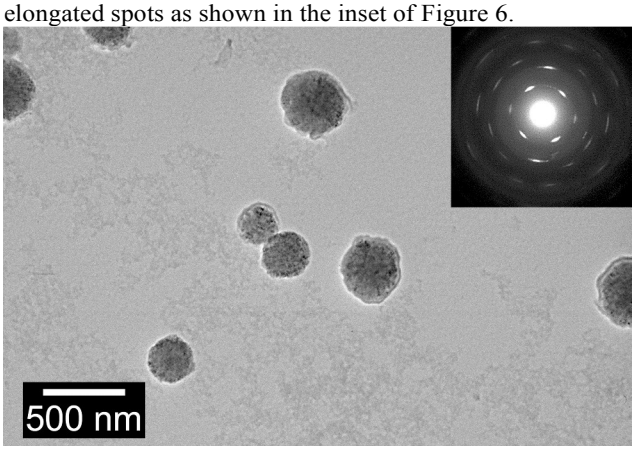

Figure 6. TEM micrograph of an extraction replica. The inset at the right hand side shows electron diffraction pattern (SAD) of single particles.

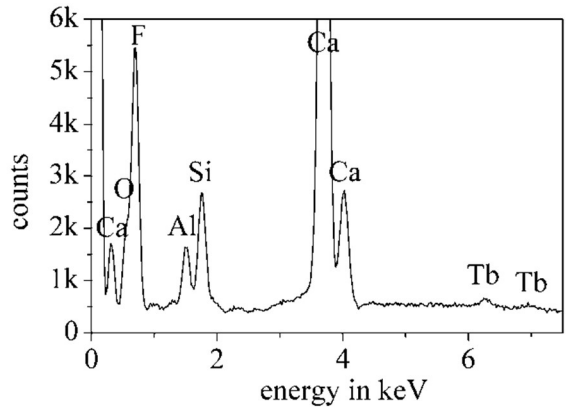

Figure 7. EDS-spectrum of one particle recorded by TEM.

The EDS-spectrum recorded from these particles shows qualitatively that the calcium and fluorine peaks are the main peaks (see Figure 7). However, there are still minor concentrations of aluminum and silicon present. Terbium is near the detection limit but still unquestionable present in the particle.

Static fluorescence emission spectra are shown in Figure 8, Figure 10 and Figure 11 for Tb^{3+}-concentrations of $1 \cdot 10^{19}$, $5 \cdot 10^{19}$ and $10 \cdot 10^{19}$ cm^{-3}, respectively. In each figure, the spectra of the glass and of samples crystallized at 580 and 600 °C for 20 h are shown. The emissions at 487, 542, 583 and 622 nm are attributed to the $^5D_4$-transitions to the $^7F_{(6,\ 5,\ 4,\ 3)}$ levels, respectively. The peaks at shorter wavelengths of 416, 436 and 458 nm are due to the $^5D_3$-transitions to the $^7F_{(6,\ 5,\ 4)}$ levels, respectively.

The emissions of the samples with the lowest Tb^{3+}-concentration ($1 \cdot 10^{19}$ cm^{-3}) are scarcely affected by the thermal treatment as shown in Figure 8. The spectra have approximately the same shape and peak intensities in the glass as well as in all crystallized samples. Figure 9 shows the fluorescence decay curves of these samples measured at the respective peak wavelengths of two emission bands, 542 nm for the transitions originating at the $^5D_4$ level and 436 nm for the $^5D_3 \rightarrow {}^7F_x$ emission band. Two groups of decay curves can be seen: one with a constant, relatively slow decay of 4.55 ms (green curves) and another with a constant but faster decay of 1.93 ms (blue curves). The first decay time is observed at a wavelength of 542 nm, the second at 436 nm. The spectra of annealed samples are quite similar. All measured lifetimes are summarized in Table 2. Interestingly, all fluorescence decay curves show a slight deviation from a mono-exponential shape (non-linear decay in half-logarithmic scale) as shown in Figure 9.

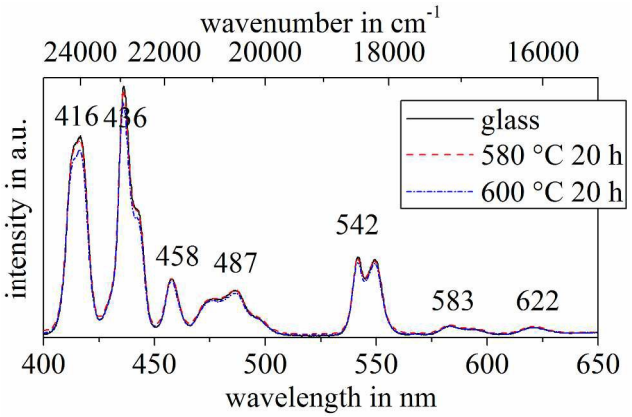

Figure 8. Fluorescence spectra of the sample A1 ($1 \cdot 10^{19}$ Tb^{3+} cm^{-3}) without and with thermal annealing at 580 and 600 °C for 20 h.

By contrast, the emission spectra shown in Figure 10 recorded from samples A5 with a Tb^{3+}-concentration of $5 \cdot 10^{19}$ cm^{-3} are strongly affected by the thermal treatment. The intensity uniformly increases with increasing annealing temperature for all observed transitions. For these samples the observed lifetimes are about 1.56 ms at 436 nm and 3.56 ms at 542 nm (see grey curves in Figure 9) and hence smaller than for the A1 samples. It should be noted that in agreement with the sample A1, the different heat treatments of sample A5 do not noticeably affect the fluorescence decay curves. For the sample A5, the decay curves at 542 nm have a perfect mono-exponential shape. The curves at 436 nm differ slightly from a mono-exponential shape which was also observed in sample A1.

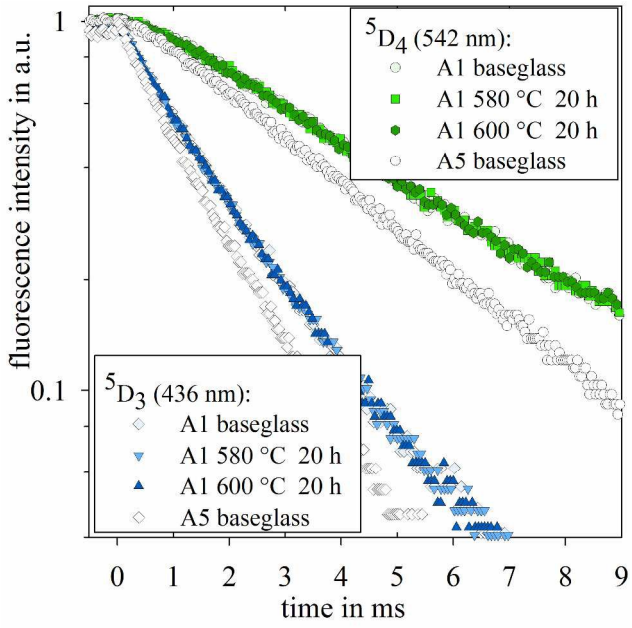

Figure 9. Fluorescence decay curves of the transitions at 436 and 542 nm for the sample A1 ($1 \cdot 10^{19}$ Tb^{3+} cm^{-3}) without and with thermal annealing as well as the glass without annealing of sample A5 ($5 \cdot 10^{19}$ Tb^{3+} cm^{-3}).

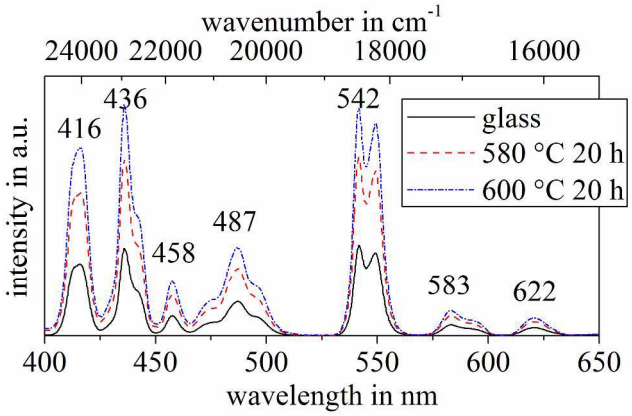

Figure 10. Fluorescence spectra of the sample A5 ($5 \cdot 10^{19}$ Tb^{3+} cm^{-3}) without and with thermal annealing at 580 and 600 °C for 20 h.

Figure 11 shows fluorescence emission spectra of sample A10 with the highest Tb^{3+}-concentration ($1 \cdot 10^{20}$ cm^{-3}). Here, the annealed samples show slightly increased fluorescence intensity in comparison to the sample without annealing. It is seen that the intensity ratio between transitions of different origin remains constant for the samples with and without annealing. However, changes of the intensity ratio can be stated, if samples with different doping concentrations are compared (Figure 8, Figure 10 and Figure 11). In Table 2, these intensity ratios of the transition $^5D_3 \rightarrow {}^7F_5$ at 436 nm and $^5D_4 \rightarrow {}^7F_5$ at 542 nm are shown. For the sample A1 with a Tb^{3+}-concentration of $1 \cdot 10^{19}$ cm^{-3}, the $^5D_3 \rightarrow {}^7F_x$ transitions possess a higher intensity than the $^5D_4 \rightarrow {}^7F_x$ transitions, for the medium doping concentration of sample A5 ($5 \cdot 10^{19}$ cm^{-3}), the intensity of both emission bands is about the same and for the highest doping concentration in sample A10 ($1 \cdot 10^{20}$ cm^{-3}), the $^5D_4 \rightarrow {}^7F_x$ transitions are generally stronger than the $^5D_3 \rightarrow {}^7F_x$ band. A similar trend of decreasing intensity ratio can be observed in the samples B without fluoride. The fluorescence lifetime measurements of sample A10 (3.54 ms at 542 nm and 1.42 ms at 436 nm) resulted in similar decay times in comparison with the samples A5. The decay of the $^5D_4 \rightarrow {}^7F_x$ transitions is mono-exponential while the decay of the $^5D_3 \rightarrow {}^7F_x$ band is not mono-exponential and the fluorescence lifetime slightly shorter than of sample A5. Again, the annealing of the samples has no influence on the fluorescence lifetimes. The decay times are summarized in Table 2.

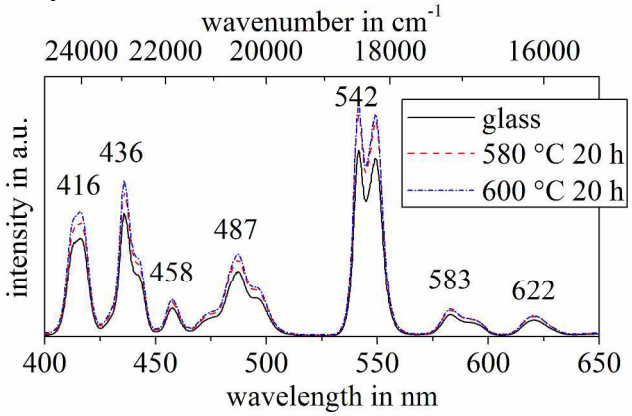

Figure 11. Fluorescence spectra of the sample A10 ($1 \cdot 10^{20}$ Tb^{3+} cm^{-3}) without and with thermal annealing at 580 and 600 °C for 20 h.

Table 2. Fluorescence decay times τ and intensity ratio for terbium doped samples. The measured lifetimes are averaged for samples of different heat treatments. The accuracy of the measurement is estimated with ±0.03 ms.

sample	intensity ratio $^5D_3$ / $^5D_4$	τ in ms at 436 nm ($^5D_3$)	τ in ms at 542 nm ($^5D_4$)
A1	3.1	1.93	4.61
A5	1.0	1.56	3.56
A10	0.6	1.42	3.54
B1	2.2	1.84	4.55
B5	1.3	1.43	3.36

Discussion

The prepared glasses without the addition of rare earth dopants show properties that are in agreement with previous studies of oxyfluoride glass-ceramics and the formation of nanocrystals [11, 19]. The fining agent Sb_2O_5 does not noticeably affect the crystallization process. As shown in Figure 3, the glass transition temperature measured by DSC from the crystallized samples increased in comparison to that of the glassy sample. The as measured temperatures are attributed to T_g of the residual glassy phase of the glass-ceramic sample. Annealing at 550 °C resulted in a T_g of 540 °C, whereas crystallizing at 580 °C led to a T_g of 560 °C. This behavior was expected and previously observed for similar glass compositions. In analogy to previous studies, this can be explained as follows: if CaF_2 crystallizes Ca^{2+} as well as F^- ions which both are network modifiers are removed from the glass composition and the viscosity increases and hence also the glass transition temperature. This happens first in the vicinity of the formed crystals and results in crystals that are surrounded by a highly viscous layer which hinders further diffusion of the crystal forming ions and therefore decelerates crystal growth. Previous studies were also carried out in dependence of annealing time and showed, that crystallizing for 20 h might not be sufficient to reach a T_g value which is independent of time, i.e. does no longer increase. It is assumed that the T_g of the residual glassy phase approaches the annealing temperature for infinitely long thermal treatment. As shown in Figure 2, the crystals have a size of approximately 12 nm, which does not depend on the crystallization temperature within the limits of error. This has also been explained by the hindered crystal growth, due to the formation of a highly viscous layer.

In the present study, the situation is more complicated if terbium is added to the glass batch. Even small concentrations of rare earth ions in the glass are known to form clusters in the glass network or liquid/liquid phase separation [24]. Also in the BaF_2-system, phase separation was observed if only 0.05 mol% SmF_3 or ErF_3 (equal to $1 \cdot 10^{19}$ cm^{-3}) was added to the glass composition [25]. A similar process can be assumed in the present CaF_2 system if terbium is added to the glass composition. For instance, the glass sample A5 shows droplet phase separation structures with sizes in the range from 30 to 40 nm. After thermal treatment of the glass, the structure is more pronounced but the crystallite size remains approximately constant for all compositions (see Figure 4). Obviously CaF_2 crystals are formed (proved by XRD) and are situated inside the former phase separation droplets. This assumption is supported by the observation in sample A5 where clearly visible large spherical particles are observed which possess a substructure (see Figure 5). Furthermore, the diameter of the droplets is around 400 nm and much larger than the crystal size calculated from the line

broadening in the XRD pattern. It is likely that these crystalline particles are formed from a liquid droplet phase which is the result of liquid/liquid phase separation. Inside these droplets enriched in calcium, fluoride and most probably terbium, the crystallization of CaF_2 takes place. The occurrence of phase separation and nanocrystals within the formed droplets was also observed recently in the LaF_3 and SrF_2 oxyfluoride system [10, 18]. However, the possibility of separating and analyzing these particles is novel in the present study. It can be stated that the droplets contain mainly CaF_2, and additionally some residual glassy phase (enriched in Si and Al as proved by EDS, see Figure 7). Obviously, this phase also forms a barrier between the CaF_2 particles which hinders the growth of larger CaF_2 crystals inside the droplets, e.g. by Ostwald ripening. Electron diffraction of the separated particles (without glass matrix) by TEM proved their poly-crystallinity. The SAD patterns do not show discrete spots, but show circular directed and elongated spots (see Figure 6). This means, the CaF_2 crystals are quite numerous, but surprisingly do not possess a statistic orientation. Otherwise, closed rings would be observed in the SAD patterns. The crystals seem to possess orientations which do not differ too much from each other. Possibly, this is due to clustering of the nanoparticles. It should be noted that XRD cannot distinguish homogeneously dispersed from clustered nanocrystals.

Another important question is whether terbium is incorporated into the crystalline CaF_2 phase. Usually this is proved by a shift of the peaks in the XRD patterns due to different lattice parameter when the rare earth ion is incorporated into the crystal lattice. In the present study the difference in ion radius of Ca^{2+} and Tb^{3+} is quite small (8 pm) and should not lead to a noticeable effect with the used experimental equipment. Another alternative is the measurement of fluorescence spectra and lifetime which might change due to the incorporation of the rare earth ion. If Tb^{3+} is mainly incorporated into a fluoride phase, the fluorescence lifetime should be increased as shown earlier for different glasses and glass ceramics and for different rare earth ions [26-29]. In fluoride rich environments fluorescence lifetimes of about 6 ms for the 542 nm band should be expected; for silicate glasses lifetimes around 3 ms are typical for this band [30]. Furthermore the shape of the emission spectra could change, for example, the width and splitting of peaks or intensity ratios [31, 32]. For this, the spectra should be compared to a reference spectra of the pure rare earth doped crystalline phase. An example for a spectrum of Tb^{3+} doped CaF_2 single crystals is given, for instance, in Ref. [33]. As can be seen, the peak at 542 nm shows a different shape in comparison to the spectra presented here. Therefore the incorporation of terbium ions into the CaF_2 crystals in the annealed samples should result in a modification of the peak shape in comparison to the samples without annealing.

Surprisingly, thermal treatment of the samples which leads to the formation of the CaF_2 crystal phase does neither seem to affect the shape of the fluorescence emission spectra nor the fluorescence intensity in such a way that incorporation of terbium into the crystalline phase is indicated. The observed intensity change for the composition A5 after different heat treatments is not indicating different incorporation of Tb^{3+} into the CaF_2 lattice but most likely attributed to amplification by light scattering which has previously been reported for other glass systems [34]. This assumption is supported by the increased opacity that can be observed visually in the annealed samples A5 as well as by the distinct microstructure with particle sizes of 400 nm observed by electron microscopy (see Figure 5 and Figure 6).

An effect of the dopant concentration on the fluorescence behavior, i.e. intensity ratio as well as fluorescence decay times, of both Tb^{3+} emission bands is observed. As the relative intensities of the two bands for glasses with increasing Tb^{3+} concentrations decrease (see Table 2), the concentration quenching of the $^5D_3$ emission band is obvious. This is an expected behavior because the $^5D_4 \rightarrow {}^7F_x$ transitions of terbium are reported to show no concentration quenching at least up to a concentration of $1 \cdot 10^{21}$ cm^{-3} while the $^5D_3 \rightarrow {}^7F_x$ transitions may show luminescence quenching at concentrations above $1 \cdot 10^{19}$ cm^{-3} [30, 35].

From Table 2 can be seen that there is a general decrease in the fluorescence decay times with increasing doping concentration for the measurements at 436 nm ($^5D_3$) due to quenching effects. Surprisingly the decay time for the measurements at 542 nm ($^5D_4$) decreases about 1.05 ms if the concentration of Tb^{3+} increases from $1 \cdot 10^{19}$ cm^{-3} (sample A1) to $5 \cdot 10^{19}$ cm^{-3} (sample A5) and remains constant within the limits of error for a further concentration increase (sample A10). Furthermore the decay curves for sample A1 at 542 nm ($^5D_4$) deviate at longer times (around 7 ms) from the mono-exponential trend while the other samples A5 and A10 show perfectly mono-exponential decays (see Figure 9). These findings indicate a fluorescence contribution of a small population of terbium ions which occupy certain sites in the glass structure with longer lifetime than in the other sites. This effect is only measurable at doping concentrations as low as $1 \cdot 10^{19}$ cm^{-3}, because otherwise the concentration of this special type of Tb^{3+} is negligible and its effect on the fluorescence decay curve is not detectable.

In order to study the effect of the phase separated fluoride phase, reference samples without fluoride have been prepared, while the molar ratios of all cations were kept constant (samples B1 and B5 with Tb^{3+} doping concentrations $1 \cdot 10^{19}$ and $5 \cdot 10^{19}$ cm^{-3}, respectively). Table 2 summarizes fluorescence decay times that are slightly smaller than for the respective fluoride containing samples but follow the same trend. With increasing Tb^{3+} concentration the decay times decrease for the measurements at 436 nm ($^5D_3$) as well as at 542 nm ($^5D_4$). Hence, the relatively large lifetime difference between samples doped with $1 \cdot 10^{19}$ cm^{-3} and $5 \cdot 10^{19}$ cm^{-3} still persists also for the samples without fluoride. Also the shape of the decay curves is mono-exponential for the B5 sample while it is not for the B1 sample. So this difference in the lifetimes and decay curve shapes must be related to structural changes in the residual glassy phase that cannot be solely attributed to phase separation or crystallization of the fluoride phase. This assumption is strengthened by the absence of any influence of annealing on the decay times. Furthermore, there is no change in the shape of the fluorescence excitation and emission curves for all samples. Therefore, it can be concluded that most likely the emission of Tb^{3+} doped CaF_2 crystals is not the main effect. There might be two explanations for this surprising result: On the one hand, the terbium ions may not be incorporated into the CaF_2 crystals although present in the fluoride rich droplet phase (see EDS-measurements in Figure 7) or they might be present in a relatively high concentration. The latter may result in a collapse of the fluorescence emission due to energy migration to quenching sites. This unusual behavior might be explained by at least two different local Tb^{3+} sites in the glass network, one with the same decay time that was found for samples with higher doping concentration (A5, A10, B5) and another with a longer decay time. In earlier publications we reported on some

unusual fluorescence decay behavior for Sm^{3+} and Eu^{3+} doped ternary strontium, barium and potassium alumino silicate glasses [36, 37]. Here, extraordinary long fluorescence lifetimes were found in comparison to other ternary alumino silicate glasses. The potassium alumino silicate glass showed the largest effect. Unfortunately, no investigations of multi-component alumino silicate glasses have been investigated so far. The addition of smaller amounts of these ions (Sr^{2+}, Ba^{2+}, K^{+}) to multi-component alumino silicate glasses are supposed to create rare earth sites of different local polarizability or symmetry affecting the fluorescence lifetime. However, the number of these sites must be small, since the effect is not measurable if the overall rare earth doping concentration is raised above a certain level. The decreasing decay time of Tb^{3+} for the $^5D_3$ emission measured at 436 nm with increasing Tb^{3+} concentration is superimposed by concentration quenching effects due to cross relaxation and other deactivation processes. The influence of alkaline and earth alkaline ions with large radius on glass topology will be a topic for future work.

Conclusions

Glasses with the molar composition 59.3 SiO_2·3.7 Al_2O_3·12.3 CaO·5.3 K_2O·9.0 Na_2O·10.4 CaF_2 were prepared and doped with different Tb^{3+} concentrations ($1\cdot10^{19}$, $5\cdot10^{19}$ and $1\cdot10^{20}$ cm^{-3}). The controlled subsequent thermal treatment at temperatures slightly above the glass transition temperature (520 to 600 °C) led to the precipitation of CaF_2 nanocrystals with sizes smaller than 20 nm. When the glass is doped with terbium, liquid/liquid phase separation in the glasses occurred. During thermal treatment, numerous small crystals are formed inside the droplet-like phase. This is due to the formation of a rigid residual glassy phase around the nanocrystals which hinders further crystal growth or ripening. The incorporation of terbium ions into the CaF_2 crystal phase was not confirmed by fluorescence measurements. Unusual decreasing fluorescence lifetimes with increasing terbium concentration are supposedly due to different sites in the glass network that are generated by alkaline and earth alkaline components with high atomic weight.

Notes and references

* Otto-Schott-Institut, Jena University, Fraunhoferstrasse 6, 07743 Jena, Germany, Phone: +49 3641 948538, Fax: +49 3641 948502, E-mail: christian.bocker@uni-jena.de

1 A. J. Kenyon, *Prog. Quantum Electron.*, 2002, 26, 225-284.
2. I. Gugov, M. Müller and C. Rüssel, *J. Solid State Chem.*, 2011, 184, 1001-1007.
3. X.-y. Sun and S.-m. Huang, *Nucl. Instrum. Methods Phys. Res., Sect. A*, 2010, 621, 322-325.
4. X. B. Chen and Z. F. Song, *Solid State Commun.*, 2005, 136, 313-317.
5. A. de Pablos-Martín, G. C. Mather, F. Muñoz, S. Bhattacharyya, T. Höche, J. R. Jinschek, T. Heil, A. Durán and M. J. Pascual, *J. Non-Cryst. Solids*, 2010, 356, 3071-3079.
6. G. Lakshminarayana, R. Yang, M. Mao, J. Qiu and I. V. Kityk, *J. Non-Cryst. Solids*, 2009, 355, 2668-2673.
7. C. Bocker and C. Rüssel, *J. Eur. Ceram. Soc.*, 2009, 29, 1221-1225.
8. Y. Yu, D. Chen, Y. Wang, F. Liu and E. Ma, *J. Non-Cryst. Solids*, 2007, 353, 405-409.
9. S. Tanabe, H. Hayashi, T. Hanada and N. Onodera, *Opt. Mater.*, 2002, 19, 343-349.
10. C. Bocker, J. Wiemert and C. Rüssel, *J. Eur. Ceram. Soc.*, 2013, 33, 1737-1745.
11. C. Rüssel, *Chem. Mater.*, 2005, 17, 5843-5847.
12. S. A. Song, D. S. Kim, H. M. Jeong and K. S. Lim, *J. Lumin.*, 2014, 152, 75-78.
13. E. Radzhabov, V. Nagirnyi, M. Kirm and E. Prosekina, *IEEE Trans. Nucl. Sci.*, 2012, 59, 2074-2078.
14. M. Czaja, S. Bodyl-Gajowska, R. Lisiecki, A. Meijerink and Z. Mazurak, *Phys. Chem. Miner.*, 2012, 39, 639-648.
15. T. Komatsu and T. Honma, *Int. J. Appl. Glass Sci.*, 2013, 4, 125-135.
16. G. H. Beall, *Glass Sci. Technol.*, 2000, 73, 3-11.
17. M. J. Dejneka, *J. Non-Cryst. Solids*, 1998, 239, 149-155.
18. A. de Pablos-Martin, A. Duran and M. J. Pascual, *Int. Mater. Rev.*, 2012, 57, 165-186.
19. C. Bocker, C. Rüssel and I. Avramov, *Int. J. Appl. Glass Sci.*, 2013, 4, 174-181.
20. A. Hoell, Z. Varga, V. S. Raghuwanshi, M. Krumrey, C. Bocker and C. Rüssel, *J. Appl. Crystallogr.*, 2014, 47.
21. V. S. Raghuwanshi, A. Hoell, C. Bocker and C. Rüssel, *CrystEngComm*, 2012, 14, 5215.
22. C. Bocker, I. Avramov and C. Rüssel, *Scr. Mater.*, 2010, 62, 814-817.
23. S. Bhattacharyya, C. Bocker, T. Heil, J. R. Jinschek, T. Höche, C. Rüssel and H. Kohl, *Nano Lett.*, 2009, 9, 2493-2496.
24. T. Schaller, J. F. Stebbins and M. C. Wilding, *J. Non-Cryst. Solids*, 1999, 243, 146-157.
25. J. R. Barros, C. Bocker and C. Rüssel, *Solid State Sci.*, 2010, 12, 2086-2090.
26. D. Ehrt, A. Herrmann and M. Tiegel, *Phys. Chem. Glasses-Eur. J. Glass Sci. Technol. Part B*, 2011, 52, 68-76.
27. X.-y. Sun, M. Gu, S.-m. Huang, X.-j. Jin, X.-l. Liu, B. Liu and C. Ni, *J. Lumin.*, 2009, 129, 773-777.
28. M. Mortier, A. Monteville, G. Patriarche, G. Maze and F. Auzel, *Opt. Mater.*, 2001, 16, 255-267.
29. L. Wetenkamp, G. F. West and H. Többen, *J. Non-Cryst. Solids*, 1992, 140, 35-40.
30. A. Herrmann and D. Ehrt, *Glass Sci. Technol.*, 2005, 78, 99-105.
31. A. Herrmann, M. Tylkowski, C. Bocker and C. Rüssel, *Chem. Mater.*, 2013, 25, 2878-2884.
32. A. Herrmann, M. Tylkowski, C. Bocker and C. Rüssel, *J. Mater. Sci*, 2013, 48, 6262-6268.
33. R. L. Amster, *J. Electrochem. Soc.*, 1970, 117, 791-794.
34. D. Ehrt, H. T. Vu, A. Herrmann and G. Völksch, *Adv. Mater. Res.*, 2008, 39-40, 231-236.
35. N. Duhamel-Henry, J. L. Adam, B. Jacquier and C. Linares, *Opt. Mater.*, 1996, 5, 197-207.
36. A. Herrmann, S. Kuhn, M. Tiegel, C. Rüssel, J. Körner, D. Klöpfel, J. Hein and M. C. Kaluza, *J. Mater. Chem. C*, 2014, 2, 4328-4337.
37. A. Herrmann, S. Kuhn, M. Tiegel and C. Rüssel, *Opt. Mater.*, 2014, 37, 293-297.